

Mixer-Fed Antenna Array With Full Scanning and Sidelobe Control

Alexander J. Mackay[✉], *Graduate Student Member, IEEE*, and George V. Eleftheriades[✉], *Fellow, IEEE*

Abstract—Conventional phased array antennas are constrained by the cost of beamforming elements that are integrated at each array element to control the amplitude and phase of radiated signals. Methods to reduce the required beamformers are typically limited in scan range and sidelobe control. Here, we report how a phased array fed with integrated mixers at each element enables full beam steering and beam shaping with a reduced number of beamformers. By feeding an antenna array with rows and columns of amplitude and phase-controlled signals, the phase-addition properties of mixers are exploited to generate the required phase profile. Compared with a conventional phased array with $N \times M$ beamformers for $N \times M$ array elements, this technique requires $N + M$ beamformers. Radiation patterns from a low-profile proof-of-concept 8×8 element transmitting array with 16 beamformers demonstrate beam scanning and sidelobe control.

Index Terms—Array, beamforming, phased array, scanning, sidelobe control.

I. INTRODUCTION

EMERGING communications and sensing systems, including 6G, satellite constellations [1], [2] high-altitude platform stations (HAPS) [3], and automotive networks, all depend upon the implementation of low-cost directional antenna systems with electronically scanned beams [4]. Utilizing phased array antennas for these new applications imposes significant challenges, however.

Many phased array applications are limited by the cost of amplitude and phase-controlling beamformers [5]. Other challenges include the maximum pin counts of beamformer integrated circuits (ICs) [6], the physical space required for integrating feed elements, the complexity of multilayer printed-circuit board (PCB) designs [4], and even the quantity of distributed control signals. These issues can constrain the feasibility of phased arrays for many applications.

Reducing the number of beamforming elements required in a phased array antenna system has, therefore, been a longstanding area of research [7], [8] with many approaches. Sparse [9], [10], thinned [11], [12], or tiled subarrays [13], [14], [15], [16], [17] reduce hardware by feeding beamformers

to a limited number of array elements, feeding multiple elements with a single beamformer or placing these elements in a judicious way. These arrays often rely on some form of optimization to determine the physical arrangement of radiating elements and a set of excitation weights for a desired sidelobe level at a particular beam angle or for a range of beam angles. These solutions are often limited in their bandwidth or scan range.

Alternatively, beamforming networks can be used to distribute phased signals from a single beamformer to multiple elements. One approach is to place beamformed sources around the perimeter of a cavity that can excite traveling waves that radiate through cavity slots at angles dictated by leaky-wave modes [18], [19], [20], [21], [22]. These methods can only scan along predetermined paths, however. Distributing row and column signals that are combined linearly and passively at each radiating element [23], [24] is another method, but phase and amplitude errors inherent to the vector summation introduce significant errors.

Integrating mixers into a beamforming scheme has been proposed as early as a 1958 patent [25], and the concept has been iterated upon in various 1-D arrays [26], [27], [28], [29], [30], [31], [32]. These arrays typically consist of series feeds that accumulate frequency-dependent phase between array elements. Increasing one frequency, while decreasing the other, changes the phasing of each element and scans a beam. These arrays require a mixer at each radiating element, but no phase shifters are needed. Additional frequency-control hardware is required, however, and modulating input frequencies increases complexity and can inhibit some communications applications.

Mixer beamforming for 2-D arrays has also been proposed [33], [34], but the known experimental results [35], [36] demonstrate limited scan range and relatively small arrays with fixed amplitude distributions. One work [35] does not report scanned beams. Another [36] functions well for the intended retrodirective application, but amplitude imbalances across the array limit the sidelobes and directivity characteristics of the array itself. Both arrays are limited to 4×4 element arrays with eight phase-controlled inputs.

Here, we report the utilization of the phase-addition properties of mixers for a 2-D antenna array with full scan control. Controlled input signals around the perimeter of the array generate the phasing required to scan a single beam to any angle. We also characterize the amplitude response of the chosen mixer to demonstrate a simple means to generate shaped beams across both principal planes simultaneously.

Received 10 July 2024; revised 3 October 2024; accepted 21 October 2024. Date of publication 1 November 2024; date of current version 5 February 2025. This work was supported by the Natural Sciences and Engineering Research Council of Canada (NSERC). (Corresponding author: Alexander J. Mackay.)

The authors are with the Edward S. Rogers Sr. Department of Electrical and Computer Engineering, University of Toronto, Toronto, ON M5S 3G4, Canada (e-mail: al.mackay@mail.utoronto.ca).

Digital Object Identifier 10.1109/TAP.2024.3486962

0018-926X © 2024 IEEE. Personal use is permitted, but republication/redistribution requires IEEE permission.
See <https://www.ieee.org/publications/rights/index.html> for more information.

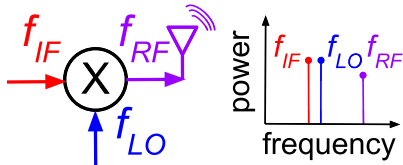


Fig. 1. Idealized mixer signal configuration.

A proof-of-concept array demonstrates a low-profile design, with the main feed implemented on a single four-layer PCB. Building upon a previous conference publication [37], we present many additional details, full beam patterns, and a comprehensive discussion of the proposed system. Compared with the existing literature, we demonstrate both full-scanning and shaped-beam functionality for the first time, with a practical and compact prototype.

The primary advantage of this array configuration is the simplified hardware configuration. While a conventional antenna array with $N \times M$ radiating elements would require $N \times M$ beamforming circuits, this array only requires $N + M$ beamformers. The advantages of a mixer-fed array, therefore, become more significant for larger arrays. The presented experiment uses an 8×8 element array controlled by 16 beamformers. The cost of including a mixer at each antenna element is significantly smaller than the cost of integrating a beamformer circuit at each element. Another advantage is that the mixers do not require individual control signals. The beamformers required by a mixer-fed array operating as an upconverting, transmitting array can operate at lower intermediate frequency (IF) and local oscillator (LO) frequencies than an identical array using beamformers at the radio frequency (RF) frequency, reducing component cost further and possibly easing fabrication tolerances.

II. MIXER BEAMFORMING

Used herein, a mixer can be conceptualized as a three-port device that multiplies an input IF signal by a reference LO signal, outputting a product RF signal. While IF, LO, and RF are all terms that describe mixer signals in a conventional heterodyning application, here, they refer to the mixer's inputs (IF and LO) and output (RF), as shown in Fig. 1. The signal multiplication will produce multiple frequency components, which is the property for which mixers are typically used. Here, the phase response of a mixer, that the phases of the inputs are added at the output, is of primary interest.

The phase relation of the upper sideband of an upconverting mixer can be written as follows:

$$\Phi_{n,m}^{RF} = \Phi_{n,m}^{LO} + \Phi_{n,m}^{IF}. \quad (1)$$

For a beam pointing in direction (θ_0, ϕ_0) , the relative phase shifts between adjacent y rows and x columns of radiating elements in a uniformly spaced antenna array will be [38]

$$\begin{aligned} \Phi_x &= -k_0 d \sin \theta_0 \cos \phi_0 \\ \Phi_y &= -k_0 d \sin \theta_0 \sin \phi_0 \end{aligned} \quad (2)$$

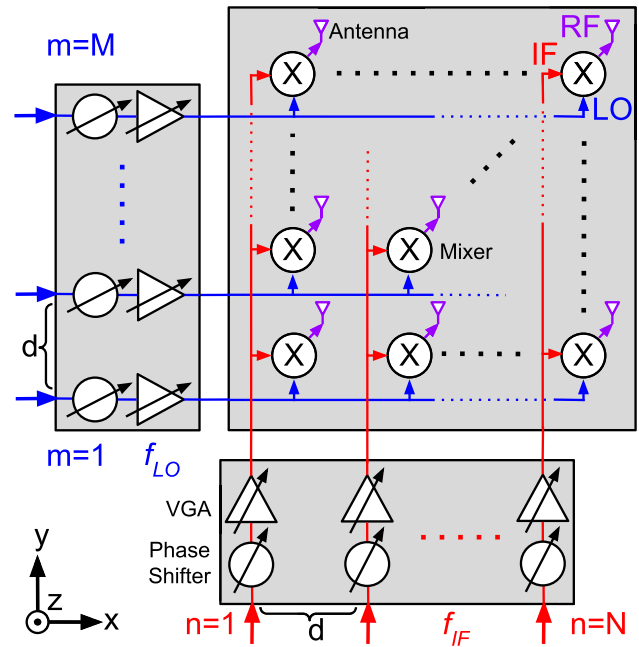


Fig. 2. Mixer array concept, showing how IF (red) and LO (blue) signals can be distributed across an array.

following the coordinate system in Fig. 2, where d is the interelement spacing and k_0 is the wavenumber at frequency f_0 . The phase at each array element will, therefore, be

$$\Phi_{n,m} = n\Phi_x + m\Phi_y. \quad (3)$$

A traditional phased array antenna will achieve this condition by generating the required phase at each radiating element independently. A less restrictive condition is to instead generate the Φ_y and Φ_x phase shifts for each row and column and combine those signals at each array element.

This phasing condition can be achieved with feeding power dividers, shown in Fig. 2, extending along each row and column of array elements, delivering the required interrow or intercolumn relative phase shifts to each element. A mixer could then combine these two signals, adding their phases and outputting RF signals with the phasing required to scan a beam to a desired angle.

For series row and column dividers, the phases at the mixer inputs (divider outputs) will be

$$\begin{aligned} \Phi_{n,m}^{IF} &= \Phi_n^{in} + \Phi_m^{col} \\ \Phi_{n,m}^{LO} &= \Phi_m^{in} + \Phi_n^{row} \end{aligned} \quad (4)$$

where Φ_n^{in} and Φ_m^{in} are the phases at the input of the IF and LO dividers and Φ_m^{col} and Φ_n^{row} are the insertion phases ($\angle S_{(m+1)1}$ or $\angle S_{(n+1)1}$) of the column and row dividers, respectively. Therefore, the required scanning condition can be achieved by setting each input phase to

$$\begin{aligned} \Phi_n^{in} &= n\Phi_x - \Phi_n^{row} \\ \Phi_m^{in} &= m\Phi_y - \Phi_m^{col}. \end{aligned} \quad (5)$$

By combining (1), (4), and (5), it is clear that (3) is satisfied, and the beam can be scanned to any angle. The series feeds

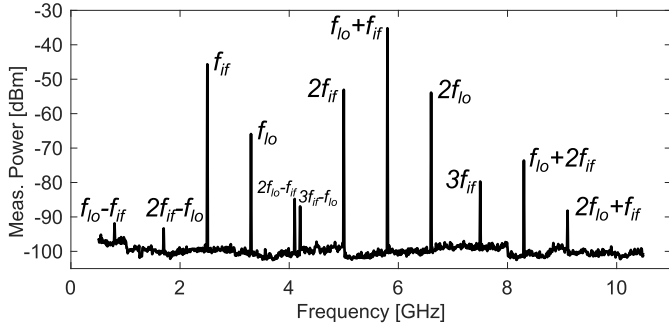


Fig. 3. Measured mixer output spectrum, with all first-, second-, and third-order products.

used here will be bandwidth-limited, as Φ_m^{col} and Φ_n^{row} phase terms will vary with frequency. A parallel feed could also be used, trading increased bandwidth for an increase in physical feed size.

III. ARRAY ARCHITECTURE

An array feed capable of supplying the phases stipulated in (5) is illustrated in Fig. 2. This proof-of-concept array comprises 8×8 radiating elements, sufficient to demonstrate shaped, directive beam patterns. The frequencies chosen for the IF, LO, and RF signals are design decisions that will depend upon the particular application. Choosing a small IF frequency will produce an output image frequency close to the desired RF, requiring a selective output filter. Closer IF and LO frequencies push the harmonic frequencies close to the upconverted RF frequency, however. IF and LO frequencies could also be chosen to further optimize component cost; reducing the IF frequency could allow for a less costly set of IF beamformers, at the possible expense of extra filter circuitry.

For the proof of concept presented here, $f_{IF} = 2.5$ GHz and $f_{LO} = 3.3$ GHz were chosen, for a transmit frequency of $f_{RF} = 5.8$ GHz. This configuration does not require any additional filters, assuming careful radiating element design. Most intermodulation products will be dissipated by the output matching network and reflected by the radiating elements. The most significant undesired frequency components are the harmonics of the input frequencies: the 5-GHz IF harmonic and 6.6-GHz LO harmonic.

A plot of the RF output spectrum of a typical array element is shown in Fig. 3. While the desired 5.8-GHz frequency is the strongest frequency component, the input IF and LO signals, as well as their harmonics, are also clearly present. These components will be somewhat filtered by the radiating elements, but could be further reduced with additional filter circuitry.

A. Feed Dividers

Sets of series-cascade unequal power dividers were designed to distribute near-equal power to each IF and LO mixer input and are shown in Fig. 4. Array performance is sensitive to feed characteristics, with power distribution levels influencing beam shape, in particular. To demonstrate the utility of this design as a low-profile phased array, both IF and LO power

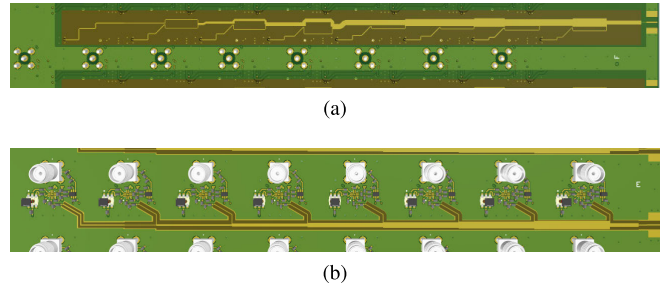


Fig. 4. Series dividers designs, in Altium. (a) IF (column) divider, designed for a 2.5-GHz center frequency on the bottom PCB layer. (b) 3.3-GHz LO (row) divider, placed on the top layer with the mixer circuits.

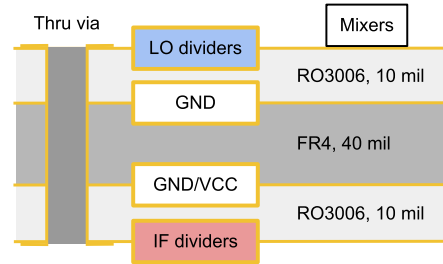


Fig. 5. Mixer-feed PCB stackup.

dividers were integrated onto a single four-layer PCB along with the mixers themselves.

The IF dividers operate with a center frequency of 2.5 GHz and are implemented as a cascade of unequal Wilkinson power dividers. The range of transmission line impedances that could be practically realized with the chosen PCB stackup and commercially available fabrication tolerances limited the power division ratios to 1:5.9, slightly less than the 1:7 ratio that would ideally be implemented as the first stage. This practically results in an insertion loss about 1 dB smaller for the first two outputs than the other six outputs.

The LO dividers operate at 3.3 GHz and are implemented as a cascade of matched T-dividers, on a PCB layer shared with the mixer layout. These dividers were designed for exactly equal output power levels. While a Wilkinson implementation would be more desirable, it would require more physical space on the PCB.

Each set of dividers can be implemented on a single PCB layer, within the uniform 25-mm array-element spacing. The higher frequency LO dividers require less physical space, which allows their implementation on the same layer as the mixer circuits. Allowing for two additional layers for ground planes and dc biasing, the entire feed can be implemented on a four-layer PCB with thru vias only. The PCB stackup used to develop the proof-of-concept array is shown in Fig. 5.

To validate the performance of the IF and LO power dividers, test boards were fabricated. Measured S-parameters are plotted in Fig. 6. The IF and LO power divider insertion losses vary from 8.7 to 10.8 dB and from 8.9 to 10.0 dB, respectively. An ideal eight-way power divider will undergo 9.0 dB of S_{11} insertion loss, so the maximum loss of an IF power divider channel is 1.8 dB, or 1.0 dB for the LO divider. Variations in output amplitude can be compensated by adjusting the beamformer amplitude at the opposing set

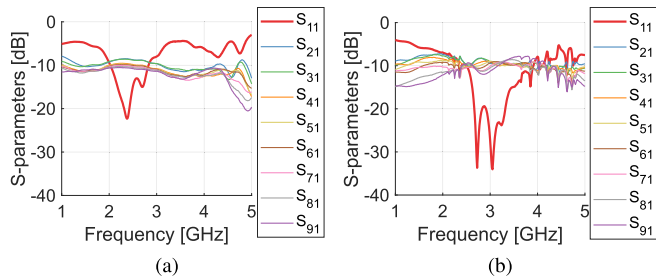


Fig. 6. (a) IF- and (b) LO-feed measured S-parameters. The IF feed is centered at 2.5 GHz, and the LO feed at 3.3 GHz.

TABLE I
MIXER LAYOUT COMPONENTS

Number	Description	Model Number
M1	Microwave Mixer	Analog Devices LTC5562
T1	Transformer	Mini-Circuits TCM1-83X+
T2	Transformer	Mini-Circuits NCS4-63+
C1-C3, C5-C12	1 nF Capacitor	Murata GRM155R71H102KA01D
C4	1 pF Capacitor	Johanson 500R07S1R0AV4T
L1	1.8 nH Inductor	CoilCraft L-07C1N8SV6T
L2, L4	3.9 nH Inductor	CoilCraft L-07C3N9SV6T
L3	1 nH Inductor	CoilCraft L-07C1N0SV6T
L5	1.5 nH Inductor	CoilCraft L-07C1N5SV6T

of feeds, given that the variations are constant across all the power dividers.

IV. MIXER CHARACTERIZATION

The LTC5562 mixer used to demonstrate the proof-of-concept array was chosen for its large bandwidth and integrated amplifier. The internal amplifier could offset the conversion loss of the mixer itself, though the net loss in our application is still positive. Some measurements were taken to verify the phase-addition and conversion loss properties needed for beamforming, which show that the chosen mixer is a practical choice for this application.

A. Mixer Layout

The chosen LTC5562 mixer requires a balanced IF input signal and outputs a balanced RF signal. It also requires external matching networks for all three IF, LO, and RF ports. Starting with the supplier-recommended networks, the matching networks were improved iteratively to account for the parasitics introduced with the employed layout. The transformers and matching networks are shown in Fig. 7(a) and listed in Table I. A 3-D render of the mixer layout, from the PCB design tool Altium, is shown in Fig. 7(b). The employed layout worked well and is replicated across all 64 mixers. The IF/RF conversion loss at the power levels used for array measurements, including the matching networks, is 4.0 dB.

B. Mixer Phase Response

Phase measurements are shown in Fig. 8(a), measured by comparing RF and reference signals with an oscilloscope. These measurements show nearly ideal output phase tracking with input phases, more than sufficient for accurate beam-forming. Any error is within the expected tolerance of the

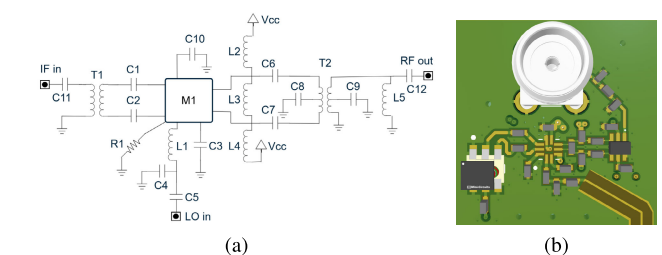


Fig. 7. (a) LTC5562 mixer schematic. (b) Mixer circuit layout, in Altium.

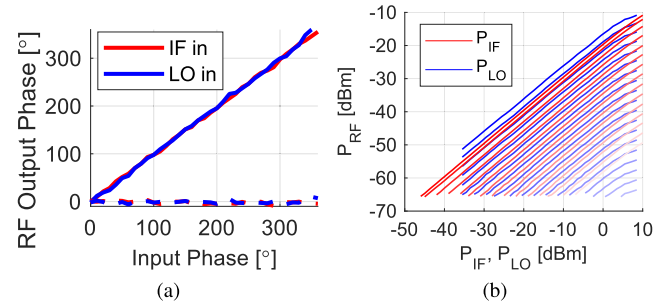


Fig. 8. (a) Mixer phase response. Measurements were taken by modulating the input IF or LO phase and comparing the RF output phase with a reference waveform. Dashed line is phase error. (b) Mixer amplitude response. Each trace plots RF output power as a function of IF power when LO power is fixed, or LO power when IF power is fixed.

oscilloscope-based phase measurements. Across both inputs, the average absolute phase error is 2.6° , and the maximum measured error is 10.0° , validating the phase-addition property experimentally.

C. Mixer Amplitude Response

By controlling the amplitudes of the signals input to the array feed, the magnitudes of the output signals can be tailored to suit a desired distribution and shape the radiated beam. Assuming equal amplitudes are delivered to each divider output, an amplitude distribution input to the rows or columns will be present, with some transformation, across each row or column of radiating elements.

The magnitude response of the LTC5562 mixer [39] is shown in Fig. 8(b), measured at one of the mixer outputs of the prototype array. Input power levels were measured at the IF and LO array inputs and are, therefore, susceptible to beamformer, divider, and conversion losses. The linear characteristics, in the dB scale, allow the mixer to be modeled as a power combiner with a fixed loss factor

$$P_{RF} [dB] = P_{LO} [dB] + P_{IF} [dB] - P_{loss} [dB]. \quad (6)$$

This model is accurate up to a 1-dB compression point of about 9 dBm of IF input power and 3 dBm of LO input power. At these power levels, the measured array channel has about 21.5 dB of loss through the array feed, mostly from the power dividers distributing power to all 64 array elements. An ideal 64-way power divider would incur 18 dB of insertion loss, however, so summing the power across all outputs would result in 3.5 dB of net loss from the beamformers, dividers, and mixer conversion. While the exact losses from each stage of the feed cannot be directly measured,

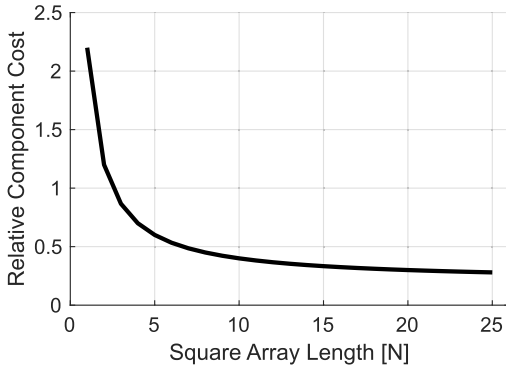


Fig. 9. Relative component cost as a function of array size. Relative cost is the component cost of an $N \times N$ element mixer-fed array (including $2N$ beamformers), divided by the cost of an array of the same size with a beamformer at each element.

test board measurements of the various stages suggest the first set of dividers, and beamformers have a small net gain due to the variable gain amplifier (VGA), about 2.0 dB. The IF series divider feed undergoes about 1.5 dB of loss, and the mixer has a conversion loss of 4.0 dB.

These power-combining characteristics allow for relative amplitude distributions to be easily realized across both the rows and columns of array elements, for simultaneous beam shaping across both principal axes. Assuming that power levels are kept below saturation, applying the well-known Chebyshev weights to the IF inputs would enforce a Chebyshev distribution across each row of elements, regardless of the input LO power across a given row. The LO inputs could be similarly tailored to enforce an amplitude distribution across each column, for simultaneous shaped beams across both the xz and yz planes.

D. Mixer Component Cost

A key advantage of mixer-fed arrays is the reduced hardware cost. In most cases, the cost of a commercially available microwave mixer IC is lower than the cost of a commercially available phase shifter IC. This can be illustrated by comparing the component cost of the proof-of-concept mixer array to the component cost of an equivalent array with independent beamformers at all 64 radiating elements. The unit cost of a mixer circuit is about 20% of the cost of a full beamformer, consisting of VGA and phase shifter ICs, including all peripheral matching, biasing, and decoupling components for both circuits. This estimate assumes commercially available components in the quantities required for a single 8×8 element array. Mixer-fed arrays still require some number of beamformers, though the number scales with the length of the array ($2N$), as opposed to the area (N^2). Also, the IF and LO beamformers used for the prototype array, which operate at 2.5 and 3.3 GHz, have a component cost of 90% of equivalent beamformers that work at the RF frequency (5.8 GHz). A plot of relative component cost as a function of array size is shown in Fig. 9. The relative component cost of the 8×8 element array is about 43% of a conventional array, and the relative cost is less than 50% for any array with 7×7 elements or more.

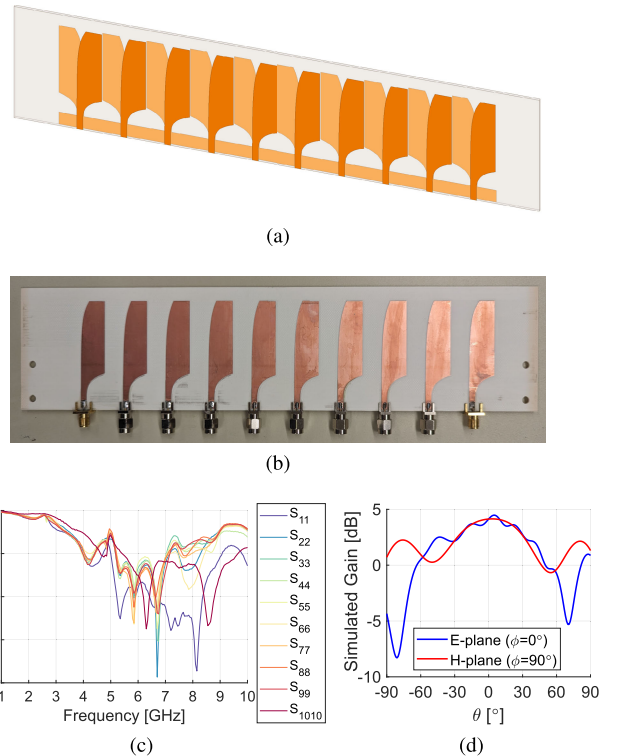


Fig. 10. (a) HFSS model of radiating elements. (b) Photograph of fabricated radiating elements. (c) Radiating element return losses, for a typical row of radiating elements. Each port is connected to a single tapered slot. The first (S_{11}) and last (S_{1010}) elements of each row are not driven, but are terminated with 50Ω loads. (d) Gain of a single tapered slot element, simulated in HFSS.

V. PROTOTYPE IMPLEMENTATION

A uniform mixer spacing of $d = 25 \text{ mm} = 0.47\lambda_0$ for the rows and columns was chosen to suppress grating lobes at the center frequency of 5.8 GHz. Each mixer's RF output connects to an SMA connector. These connectors have the same uniform 25-mm spacing, which allows for integration with radiating elements or direct measurement of each mixer's output.

A. Radiating Element

Radiating elements are implemented as tapered slots, due to their flexibility in realizing the desired bandwidth [40] and physical integration with SMA connectors that easily connect to the array feed.

The array elements were implemented as tapered slots on a two-layer PCB. This allowed the elements to be easily integrated with the feed through SMA connectors, improving the modularity of the proof of concept. The elements were fabricated on eight separate two-layer PCBs. Rogers RO4003c was used as a substrate material. Passive elements were added to the beginning and end of each row, and terminated with 50Ω loads, which has the effect of stabilizing the element factors of the first and last driven elements. Fig. 10 shows simulated radiation patterns and measured return loss plots.

B. Beamformers

Beamformers are required to control the amplitude and phase of each input; 16 total beamformers are needed for the

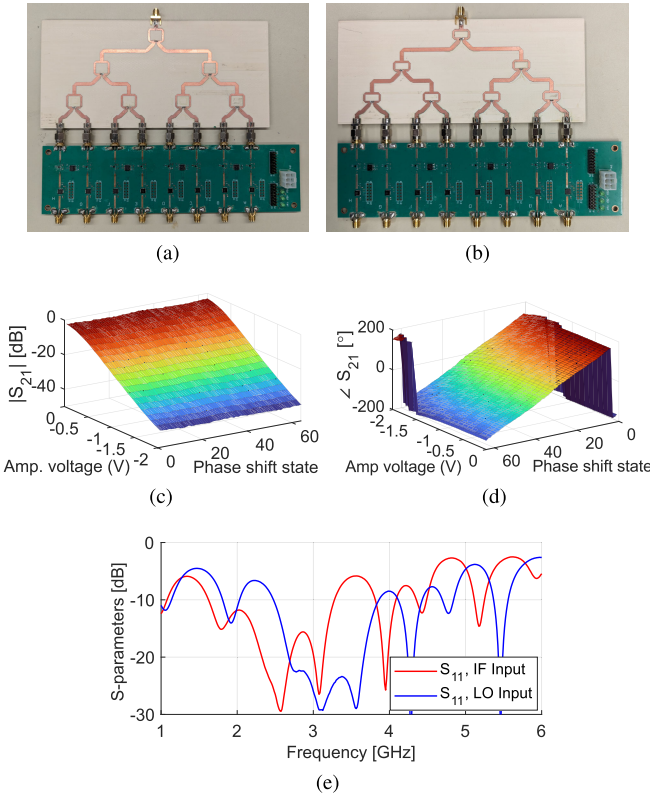


Fig. 11. Photographs of (a) IF and (b) LO beamformer boards. Measured (c) amplitude and (d) phase responses of a typical beamformer channel, at 2.5 GHz. The phase shifter shifts through 64 discrete states, while the VGA is controlled by an analog dc voltage. (e) Measured matching at IF and LO input ports.

8×8 element array. Each beamformer channel consists of a VGA [41] and a digital phase shifter [42]. Both components can operate at the IF (2.5 GHz) and LO (3.3 GHz) frequencies. The VGA is able to supply about 30 dB of dynamic amplitude range at the chosen frequencies, and the phase shifter can provide 6-bit digital phase control in 5.6° increments. Two beamformer boards were fabricated for the IF and LO inputs, each with eight channels. The boards were fabricated as four-layer PCBs using RO4003c as a substrate material. Three-stage Wilkinson power dividers in a corporate-feed arrangement were fabricated on separate boards to produce eight equal-power signals to be input to the beamformer boards. S_{21} measurements taken with a VNA across many combinations of VGA and phase shifter states served as a basis for calibration, to account for the amplitude response of the phase shifter and the phase response of the amplifier. A script then realizes a desired amplitude and phase by interpolating a stored lookup table unique to each channel. Photographs and additional plots showing a typical beamformer's synthesis space are shown in Fig. 11. Losses through a typical channel are around 7.0 dB at the VGA's maximum gain level, leaving 2.0 dB of net gain after subtracting the 9-dB power division to the eight channels. Matching performance at the IF and LO inputs is shown in Fig. 11(e). The 10-dB return loss bandwidth is 67% for the IF input (centered at 2.5 GHz) and 44% for the LO input (centered at 3.2 GHz).

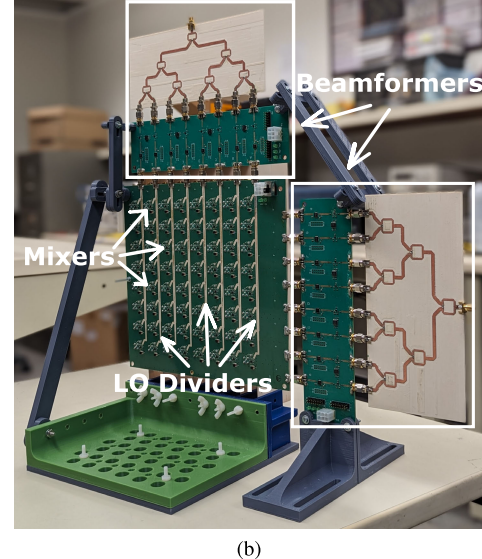
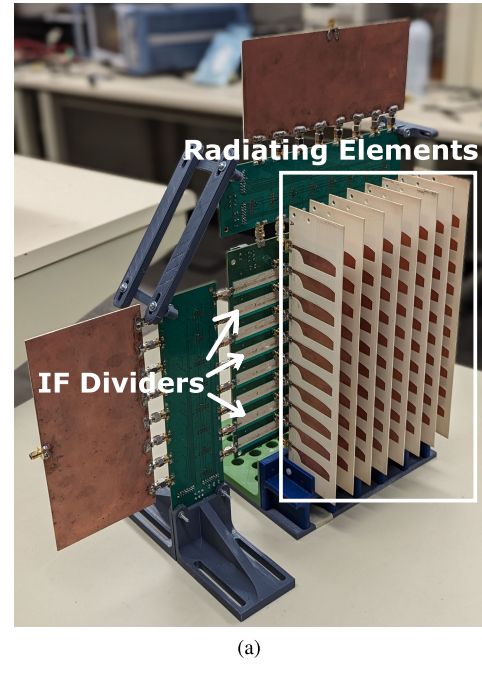


Fig. 12. (a) Front and (b) back of assembled array prototype.

VI. ARRAY CALIBRATION AND MEASUREMENT

Photographs of the assembled mixer and beamformer PCBs are shown in Fig. 12. Whenever possible, array components were fabricated on separate boards to improve modularity, but a similar system could easily be made more integrated. The 16 beamformer channels draw 6 W of dc power, mostly to the VGA. The chosen mixers include an internal amplifier to partially offset conversion losses, which results in the 64 mixers drawing about 7 W of power. Passive mixers could be used to reduce this dc draw, or additional amplification stages could be incorporated to improve system gain.

The antenna was calibrated by recording the relative output phase and magnitude of each RF output when the input beamformers were set to output a known, previously calibrated signal. Outputs were measured with a VNA, through a refer-

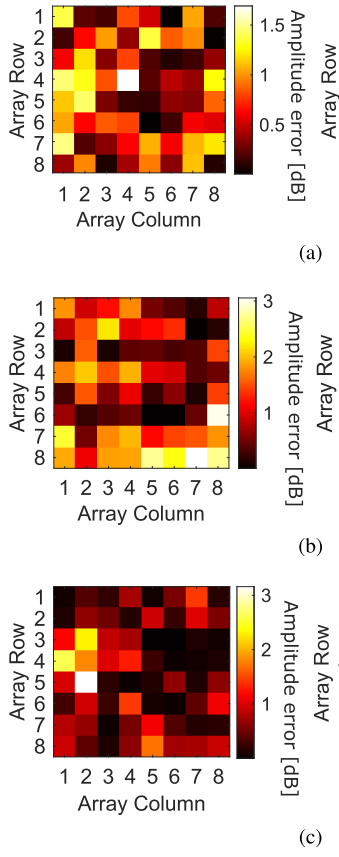


Fig. 13. (a) Measured absolute amplitude and phase error, for a uniform, broadside ($\theta = 0^\circ, \phi = 0^\circ$) excitation. (b) Measured absolute amplitude and phase error, for a uniform ($\theta = -90^\circ, \phi = 0^\circ$) excitation. (c) Measured absolute amplitude and phase error, for a 25-dB SLL, broadside ($\theta = 0^\circ, \phi = 0^\circ$) excitation.

ence mixer. The relative phase shifts were then averaged with their neighbors to obtain a set of interrow and intercolumn phase shifts, which are equal to the Φ_m^{row} and Φ_n^{col} constants from (4).

Fig. 13(a) shows the absolute phase error at each output for a typical array excitation. The worst case error of 15.4° and an average absolute error of 6.7° can be attributed to measurement and VNA calibration error and are sufficient for beam scanning.

Relative magnitudes were also measured at each output. As could be expected for any physical device with real component tolerances and hand-soldered connections, there was some variation across outputs. Variation was minimized for all measured beams by assuming the linear power-combination relationship in (6) and solving for a set of beamforming input amplitudes that minimizes the least-squared error with the desired amplitude distribution. Fig. 13(a) shows the absolute amplitude error at each output for a uniform, broadside beam. The maximum error of the uniform, broadside beam was 1.69 dB with a mean absolute error of 0.65 dB .

These measurements were also useful to quantify the feed losses. Summing the output signal amplitudes and adjusting for reference mixer loss give a total loss of 3.1 dB through the array, when the VGA amplifiers are all set to their maximum output. This roughly agrees with the 3.5-dB loss measured

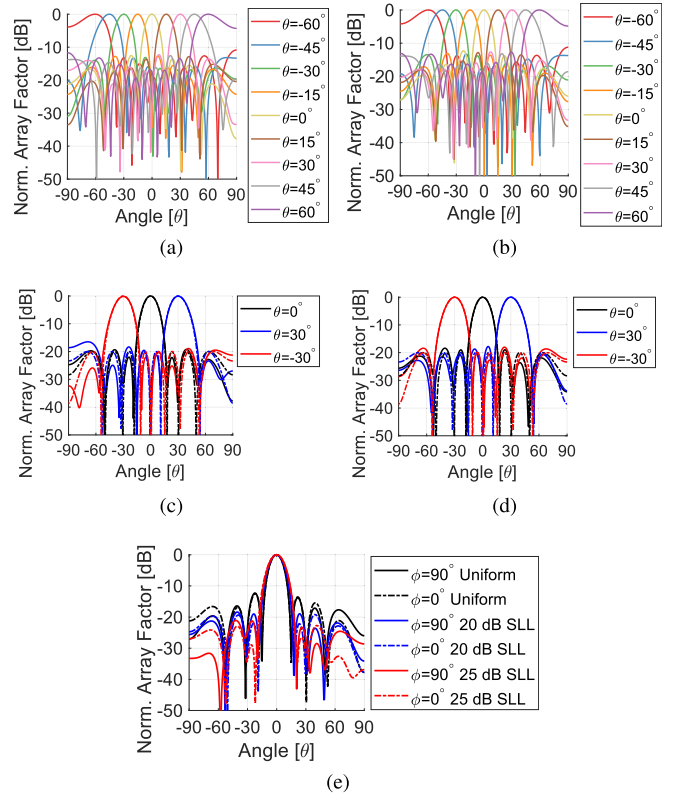


Fig. 14. Array factors, measured directly from mixer outputs, showing uniform scanned beams in (a) $\phi = 0^\circ$ and (b) $\phi = 90^\circ$ planes, 20-dB scanned Chebyshov beams in (c) $\phi = 0^\circ$ and (d) $\phi = 90^\circ$ planes, and (e) broadside shaped-beam patterns.

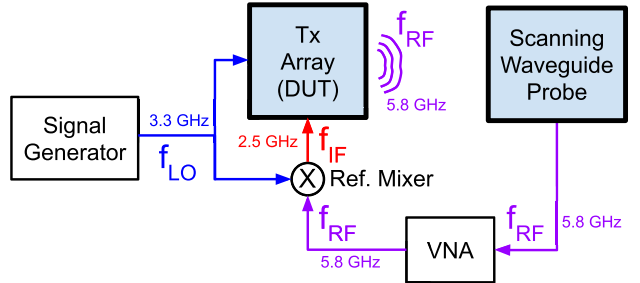


Fig. 15. Sketch of near-field scanner setup.

at a single channel in Section IV-C, within the reasonable amplitude variations across different channels of the array. Adjusting the VGAs can compensate for these amplitude variations and allow for tapered amplitude distributions across the array, at the expense of additional system losses caused by reduced VGA gains. For example, the calibrated uniform broadside beam was set without consideration of VGA or system gain and has a total feed loss of 9.0 dB .

Wider angle beam scans demonstrate the reliability of this array-phasing scheme. Fig. 13(b) of a ($\theta = -90^\circ, \phi = 0^\circ$) uniform scanned beam has a mean phase error of 7.8° and a max phase error of 30° , which is a clear outlier. The mean amplitude error of 1.1 dB and a max error of 3.1 dB are larger than the uniform broadside case that was used for calibration, but would still produce an acceptable array factor.

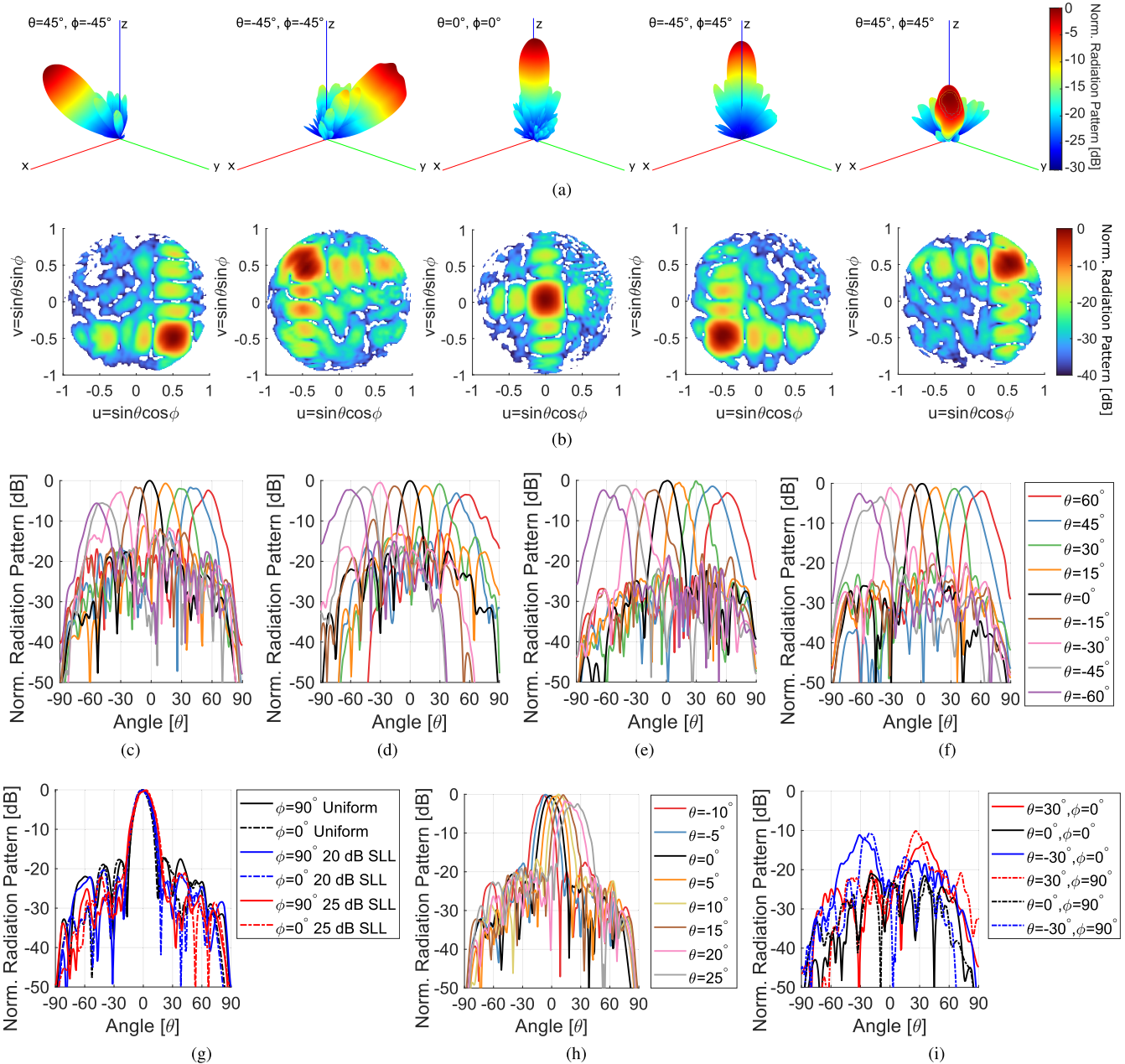


Fig. 16. Measured off-axis and broadside (a) 3-D and (b) uv-space beam plots. Uniform scanned beams in (c) E-plane ($\phi = 0^\circ$), (d) H-plane ($\phi = 90^\circ$), (e) $+D$ -plane ($\phi = 45^\circ$), and (f) $-D$ -plane ($\phi = -45^\circ$). (g) Broadside shaped beams across both principal planes. (h) Scanned E-plane ($\phi = 0^\circ$) beams with 20-dB sidelobe levels. (i) Cross-polarized radiation patterns, relative to co-polarized peaks.

Similarly, the magnitude and phase errors for a 25-dB Chebyshev distribution are plotted in Fig. 13(c). The mean absolute phase error of 5.8° and an absolute phase error of 21.3° are similar to the uniform case. The mean amplitude error was found to be 0.7 dB, and the maximum absolute error is 3.2 dB, similar to the other beam states.

Given this set of phase and amplitude adjustments, the array can be set to scan a shaped beam to any angle. While plots of errors at each output demonstrate the accuracy of the measured feed, the measured complex outputs can also be used to construct array factors, which demonstrate scanned and shaped beams without element factor or mutual coupling effects. These array factors are plotted in Fig. 14.

VII. ARRAY PATTERN MEASUREMENTS

Beam patterns were measured with an NSI 2000 near-field scanner system. The antenna under test (AUT) acted as a transmitter, and a WR187 open-ended waveguide probe received the transmitted signal. The waveguide probe was scanner to sample the array's near field, which was then converted to far-field radiation patterns. A Mini-Circuits SIM-73L+ [43] reference mixer downconverted the 5.8-GHz input signal to 2.5 GHz, which was then input to the IF beamformer boards. A diagram of the test setup is shown in Fig. 15.

As with any antenna array, the results are influenced by the characteristics of the radiating elements. While the array feed can generate the phasing needed to scan a beam to any

angle, measured radiated patterns are practically limited to a maximum scan of roughly $\theta = \pm 60^\circ$ due to mutual coupling effects.

The 3-D beam patterns and plots in uv space are shown in Fig. 16(a) and (b) and demonstrate the off-axis performance of various scanned beams. Radiation patterns of scanned beams across the E-, H-, and both D-planes are also shown in Fig. 16, demonstrating directive beams across a large scan range. Apart from some gain variation in the $-\theta$ region of the E-plane, beams can be scanned to an angle of $\theta = 60^\circ$ for most ϕ planes, after which the mutual coupling and element-factor effects degrade the radiation performance.

Observed ripples in the radiation patterns at large scan angles were not present in the measured array factors (see Fig. 14) and can, therefore, be attributed to a combination of the radiating elements and measurement system. Some ripples are seen in the simulated element-level radiation patterns in Fig. 10(d), but at these angles, fields sampled by the scanner would also be at the edges of its scan range and susceptible to measurement error.

The near-field scanner system could measure a system gain relative to a standard gain horn, which was used to infer the realized gain of the tapered slot antenna elements for a uniform, broadside beam. Subtracting losses in the reference mixer, the system gain of 13.0 dB allows for 22.0 dB of realized gain from the antenna array elements, given the 9.0 dB of loss through the feed network measured in Section VI. These feed network losses are expected and could be reduced by increasing the VGA gain at the expense of amplitude imbalances across the array. Given the 22-dB realized gain and 22.4-dB measured directivity, the radiating elements themselves have an estimated overall efficiency of 89%. The LO input power level is set to 3.0 dBm, and the IF input reference mixer limits the IF input power to 0 dBm.

The largest sidelobe measured at broadside is 17 dB below the main lobe, though sidelobe levels are larger at other scan angles. Sidelobe variations with scan angle are likely caused by radiating element and measurement effects, as the measured array factors shown in Fig. 14 demonstrate consistent sidelobe levels of about 12 dB across the scan ranges of both principal planes.

Beams with controlled sidelobe levels are shown in Fig. 16(g). The mutual coupling effects of scanned beams degrade the sidelobe performance away from broadside, but 20-dB sidelobe distributions perform well from $\theta = -10^\circ$ to $\theta = 25^\circ$ in the E-plane, and are plotted in Fig. 16(h). Patterns with sidelobes as small as -25 dB, measured simultaneously across the E- and H-planes, were measured at broadside and are plotted in Fig. 17. Measured array factors do not suffer from radiating element effects, and plots in Fig. 14 show accurate controlled sidelobe beam scanning across both principal axes.

A. Radiation Pattern Bandwidth

As the IF and LO feeds are implemented as series dividers, the radiated beam will naturally scan along the axes of these dividers as frequency is varied, limiting the bandwidth. This property could be used as a scanning mechanism for

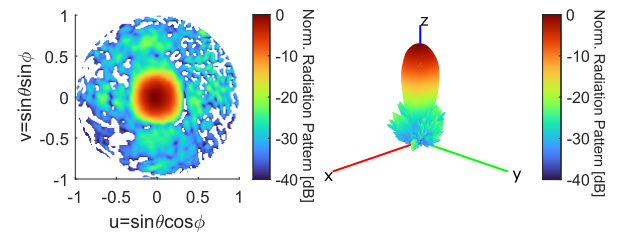


Fig. 17. Measured radiation pattern of a 25-dB SLL-shaped beam at broadside.

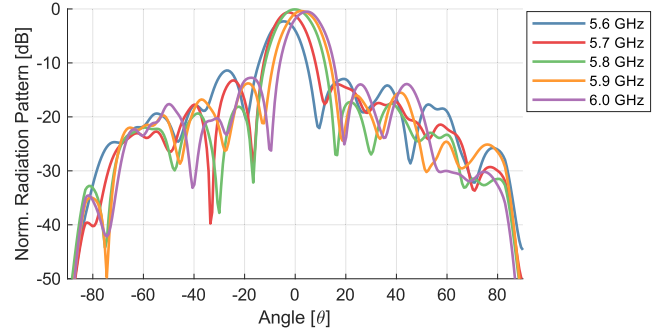


Fig. 18. Measured broadside, uniform pattern bandwidth. As IF frequency is varied, the RF frequency will change, and the radiated beam scans along the H-plane ($\phi = 90^\circ$).

some applications, replacing the discrete phase shifters at the expense of additional frequency-control hardware. The presented proof-of-concept array will scan along the H-plane ($\phi = 90^\circ$) as the IF frequency is varied, for example. Setting the beamformers for a uniform, broadside beam at 5.8 GHz, radiation patterns at various frequencies are plotted in Fig. 18. The 3-dB bandwidth of the uniform broadside pattern is 7%. The frequency-dependent phase could be compensated for a new center frequency, however, within the bandwidth limits of the dividers themselves.

VIII. CONCLUSION

This work establishes mixer-fed arrays as a compelling architecture for phased array applications requiring reduced cost and complexity. Measured radiation patterns show how mixer-fed phased arrays can realize full beam scanning and beam shaping with a reduced number of beamformers. The proof-of-concept array has been implemented on a single four-layer PCB with commercially available components, demonstrating the practicality and simplicity of the design. The 8×8 element prototype array is larger than the 4×4 element arrays demonstrated to date [35], [36], approaching the practical limit of unequal power dividers easily integrated onto a single PCB layer. Still larger arrays could be implemented, however, with the use of modular subarrays of mixer-fed elements.

The losses inherent to mixer operation are a drawback of this approach but are mitigated in this work with the use of commercially available active mixers and VGAs. The 3.1-dB insertion loss through the network is, therefore, much smaller than the 25.8 dB seen in an earlier implementation [36]. Beamformers implemented with VGAs and phase shifters allow for corrections to amplitude imbalances across

the array, control over beam sidelobes, and full beam scanning, resulting in better sidelobe performance and scan range than found in previous works [35], [36]. Compared with a traditional array, additional amplification (and additional dc power draw) could be necessary to compensate for the mixer losses, though any traditional phased array would also include a frequency-converting mixer (e.g., for upconverting in the Tx mode) whose conversion losses might not be considered part of phased array performance.

Undesired frequency products are another drawback of this approach, though careful radiating element design and/or dedicated filters could be implemented to comply with the allowed spectrum limits of any particular application. The array demonstrated in this work operates in the transmitting mode only, but a receiving array could be implemented similarly. The receiving mixer's noise characteristics would have to be carefully considered, however.

On the other hand, mixer-fed arrays do not intrinsically suffer from the scan range or sidelobe-level limitations inherent to other reduced-beamformer arrays and can be designed and implemented without the use of computational optimization. The beamformers used for this particular implementation of a mixer array eliminate the need for a frequency-dependent phasing scheme, which requires additional specialized hardware. Future work could establish methods of generating multiple beams or exploit nonreciprocal properties of mixers for element-level in-band full-duplex antenna systems.

REFERENCES

- [1] O. Kodheli et al., "Satellite communications in the new space era: A survey and future challenges," *IEEE Commun. Surveys Tuts.*, vol. 23, no. 1, pp. 70–109, 1st Quart., 2021.
- [2] S. Liu et al., "LEO satellite constellations for 5G and beyond: How will they reshape vertical domains?" *IEEE Commun. Mag.*, vol. 59, no. 7, pp. 30–36, Jul. 2021.
- [3] M. Geen, "E-band mmWave technology for HAPS and LEO satellite systems," *Microw. J.*, vol. 64, no. 2, pp. 22–36, Feb. 2021.
- [4] T. Chaloun et al., "Electronically steerable antennas for future heterogeneous communication networks: Review and perspectives," *IEEE J. Microw.*, vol. 2, no. 4, pp. 545–581, Oct. 2022.
- [5] J. S. Herd and M. D. Conway, "The evolution to modern phased array architectures," *Proc. IEEE*, vol. 104, no. 3, pp. 519–529, Mar. 2016.
- [6] B. Sadhu, X. Gu, and A. Valdes-Garcia, "The more (antennas), the merrier: A survey of silicon-based mm-wave phased arrays using multi-IC scaling," *IEEE Microw. Mag.*, vol. 20, no. 12, pp. 32–50, Dec. 2019.
- [7] P. Rocca, G. Oliveri, R. J. Mailloux, and A. Massa, "Unconventional phased array architectures and design methodologies—A review," *Proc. IEEE*, vol. 104, no. 3, pp. 544–560, Mar. 2016.
- [8] S. Skobelev, "Methods of constructing optimum phased-array antennas for limited field of view," *IEEE Antennas Propag. Mag.*, vol. 40, no. 2, pp. 39–50, Apr. 1998.
- [9] R. M. Leahy and B. D. Jeffs, "On the design of maximally sparse beamforming arrays," *IEEE Trans. Antennas Propag.*, vol. 39, no. 8, pp. 1178–1187, Aug. 1991.
- [10] A. Trucco and V. Murino, "Stochastic optimization of linear sparse arrays," *IEEE J. Ocean. Eng.*, vol. 24, no. 3, pp. 291–299, Jul. 1999.
- [11] M. G. Bray, D. H. Werner, D. W. Boeringer, and D. W. Machuga, "Optimization of thinned aperiodic linear phased arrays using genetic algorithms to reduce grating lobes during scanning," *IEEE Trans. Antennas Propag.*, vol. 50, no. 12, pp. 1732–1742, Dec. 2002.
- [12] R. L. Haupt, "Thinned arrays using genetic algorithms," *IEEE Trans. Antennas Propag.*, vol. 42, no. 7, pp. 993–999, Jul. 1994.
- [13] B. Rupakula, A. H. Aljuhani, and G. M. Rebeiz, "Limited scan-angle phased arrays using randomly grouped subarrays and reduced number of phase shifters," *IEEE Trans. Antennas Propag.*, vol. 68, no. 1, pp. 70–80, Jan. 2020.
- [14] F. Yang, Y. Ma, Y. Chen, S. Qu, and S. Yang, "A novel method for maximum directivity synthesis of irregular phased arrays," *IEEE Trans. Antennas Propag.*, vol. 70, no. 6, pp. 4426–4438, Jun. 2022.
- [15] W. Dong, Z.-H. Xu, X.-H. Liu, L.-S.-B. Wang, and S.-P. Xiao, "Irregular subarray tiling via heuristic iterative convex relaxation programming," *IEEE Trans. Antennas Propag.*, vol. 68, no. 4, pp. 2842–2852, Apr. 2020.
- [16] J. T. Nemit, "Network approach for reducing the number of phase shifters in a limited scan phased array," U.S. Patent 3 803 625, Apr. 9, 1974.
- [17] R. Fante, "Systems study of overlapped subarrayed scanning antennas," *IEEE Trans. Antennas Propag.*, vol. AP-28, no. 5, pp. 668–679, Sep. 1980.
- [18] K. A. Oyesina and A. M. H. Wong, "Metasurface-enabled cavity antenna: Beam steering with dramatically reduced fed elements," *IEEE Antennas Wireless Propag. Lett.*, vol. 19, no. 4, pp. 616–620, Apr. 2020.
- [19] K. A. Oyesina and A. M. H. Wong, "Experimental demonstration of the metamaterial-based beam-steerable Huygens' box antenna with dramatically reduced phasing elements," in *Proc. IEEE Int. Symp. Antennas Propag., USNC-URSI Radio Sci. Meeting (AP-S/URSI)*, Jul. 2022, pp. 1852–1853.
- [20] A. H. Dorrah and G. V. Eleftheriades, "Peripherally excited phased array architecture for beam steering with reduced number of active elements," *IEEE Trans. Antennas Propag.*, vol. 68, no. 3, pp. 1249–1260, Mar. 2020.
- [21] A. H. Dorrah and G. V. Eleftheriades, "Experimental demonstration of peripherally-excited antenna arrays," *Nature Commun.*, vol. 12, pp. 1249–1260, Oct. 2021.
- [22] A. J. Mackay and G. V. Eleftheriades, "Power pattern synthesis with peripherally excited phased arrays," *IEEE Trans. Antennas Propag.*, vol. 71, no. 8, pp. 6390–6398, Aug. 2023.
- [23] D. J. Legare, "Steerable phased array antenna," U.S. Patent 10 897 082 B1, Jan. 19, 2021.
- [24] V. Mirafab and W. Zhai, "Overlapping linear sub-array for phased array antennas," U.S. Patent 10 320 087 B2, Jun. 11, 2019.
- [25] W. Welty, "Apparatus for generating plurality of signals having variable phase difference," U.S. Patent 3 090 928, Jan. 2, 1958.
- [26] M. Kim, J. Hacker, A. Sailer, and J. Hong, "A heterodyne-scan phased-array antenna," *IEEE Microw. Guided Wave Lett.*, vol. 9, no. 12, pp. 535–537, Dec. 1999.
- [27] K. Aamo, "Frequency controlled antenna beam steering," in *IEEE MTT-S Int. Microw. Symp. Dig.*, vol. 3, May 1994, pp. 1549–1552.
- [28] T. Nishio, H. Xin, Y. Wang, and T. Itoh, "A frequency-controlled active phased array," *IEEE Microw. Wireless Compon. Lett.*, vol. 14, no. 3, pp. 115–117, Mar. 2004.
- [29] T. Nishio, Y. Wang, and T. Itoh, "A frequency-controlled beam-steering array with mixing frequency compensation for multichannel applications," *IEEE Trans. Antennas Propag.*, vol. 52, no. 4, pp. 1039–1048, Apr. 2004.
- [30] J. D. Roque, G. S. Shiroma, and W. A. Shiroma, "A full-duplex, single-frequency-controlled phased array," in *IEEE MTT-S Int. Microw. Symp. Dig.*, Jun. 2006, pp. 453–456.
- [31] Y. Liu, R. Zhu, and Q. Liu, "A novel low-cost frequency diverse array with mirrored two-wave mixing," *IEEE Microw. Wireless Technol. Lett.*, vol. 33, no. 3, pp. 359–362, Mar. 2023.
- [32] R. Zhu, Y. Liu, B. Wang, W. Zhang, Q. Xu, and Q. Liu, "Frequency-controlled fixed-RF beam-steering array based on two-wave mixing with cascaded unequal power divider," *IEEE Trans. Antennas Propag.*, vol. 71, no. 2, pp. 1993–1998, Feb. 2023.
- [33] R. Mailloux, P. Caron, and F. LaRusso, "An array phasing device which uses only one phase shifter for each direction of scan," *IEEE Trans. Antennas Propag.*, vol. AP-16, no. 2, pp. 258–260, Mar. 1968.
- [34] E. Muehldorf, "Self-steered retrodirective arrays with amplification," *IEEE Trans. Antennas Propag.*, vol. AP-17, no. 1, pp. 42–49, Jan. 1969.
- [35] M. Sanchez-Barbety and R. W. Jackson, "Architecture for low cost electronically steered phased arrays," in *IEEE MTT-S Int. Microw. Symp. Dig.*, Jun. 2008, pp. 695–698.
- [36] M. K. Watanabe, R. N. Pang, B. O. Takase, J. M. Akagi, G. S. Shiroma, and W. A. Shiroma, "A 2-D phase-detecting/heterodyne-scanning retrodirective array," *IEEE Trans. Microw. Theory Techn.*, vol. 55, no. 12, pp. 2856–2864, Dec. 2007.

- [37] A. J. Mackay and G. V. Eleftheriades, "Mixer-fed antenna array for shaped beam scanning with reduced beamformers," in *Proc. IEEE Int. Symp. Antennas Propag. INC/USNC-URSI Radio Sci. Meeting (APS/INC-USNC-URSI)*, Jul. 2024, pp. 2501–2502.
- [38] C. Balanis, *Antenna Theory: Analysis and Design*, 4th ed. Hoboken, NJ, USA: Wiley, 2016.
- [39] (2017). *LTC5562 Wideband Low Power Active Mixer*. Analog Devices. [Online]. Available: <https://www.analog.com/media/en/technical-documentation/data-sheets/5562f.pdf>
- [40] W. F. Croswell, T. Durham, M. Jones, D. Schaubert, P. Friederich, and J. G. Maloney, "Wideband arrays," in *Modern Antenna Handbook*, C. A. Balanis, Ed. Hoboken, NJ, USA: Wiley, 2008, ch. 12, pp. 581–629.
- [41] *MAAM-011100 Broadband Variable Gain Amplifier*. MACOM, rev. V3. Accessed: Apr. 16, 2024. [Online]. Available: <https://cdn.macom.com/datasheets/MAAM-011100.pdf>
- [42] *MAPS-010164 Digital Phase Shifter*. MACOM, rev. V3. Accessed: Apr. 16, 2024. [Online]. Available: <https://cdn.macom.com/datasheets/MAPS-010164.pdf>
- [43] (2008). *SIM-73L+ Frequency Mixer*. Mini-Circuits. Accessed: Apr. 16, 2024. [Online]. Available: <https://www.minicircuits.com/pdfs/SIM-73L+.pdf>



Alexander J. Mackay (Graduate Student Member, IEEE) received the B.Eng. degree in electrical engineering from the Memorial University of Newfoundland, St. John's, NL, Canada, in 2017, and the M.A.Sc. degree in electrical engineering from the University of Toronto, Toronto, ON, Canada, in 2021, where he is currently pursuing the Ph.D. degree.

His research interests include phased array feeds, beam synthesis techniques, leaky-wave antennas, and radar systems.



George V. Eleftheriades (Fellow, IEEE) received the M.S.E.E. and Ph.D. degrees in electrical engineering from the University of Michigan, Ann Arbor, MI, USA, in 1989 and 1993, respectively.

From 1994 to 1997, he was with the Swiss Federal Institute of Technology, Lausanne, Switzerland. He is currently a Professor with the Department of Electrical and Computer Engineering, University of Toronto, Toronto, ON, Canada, where he holds the Canada Research/Velma M. Rogers Graham Chair in nanostructured and microstructured electromagnetic materials. He is also a Recognized International Authority and a Pioneer in the area of metamaterials. These are man-made materials, which have electromagnetic properties not found in nature. He has introduced a method for synthesizing metamaterials using loaded transmission lines. Together with his graduate students, he has provided the first experimental evidence of imaging beyond the diffraction limit and pioneered several novel antennas and microwave components using these transmission-line-based metamaterials. His research has impacted the field by demonstrating the unique electromagnetic properties of metamaterials, used in lenses, antennas, and other microwave and optical components to drive innovation in fields, such as wireless and satellite communications, defense, medical imaging, microscopy, and automotive radar. He has been leading a group of graduate students and researchers in the areas of electromagnetic and optical metamaterials; metasurfaces, antennas, and components for broadband wireless communications; novel antenna beam-steering techniques; far-field superresolution imaging; radars; plasmonic and nanoscale optical components; and fundamental electromagnetic theory.

Dr. Eleftheriades has been a fellow of the Royal Society of Canada since 2009. He has served as a member for the IEEE AP-Society Administrative Committee (AdCom) from 2007 to 2012 and an IEEE AP-S Distinguished Lecturer from 2004 to 2009. He was a recipient of numerous awards, such as the Ontario Premier's Research Excellence Award and the University of Toronto's Gordon Slemon Award in 2001, the E. W. R. Steacie Fellowship from the Natural Sciences and Engineering Research Council of Canada in 2004, the 2008 IEEE Kiyo Tomiyasu Technical Field Award, the 2009 Best Paper Award from IEEE ANTENNAS AND WIRELESS PROPAGATION LETTERS, twice the R. W. P. King Best Paper Award from the IEEE TRANSACTIONS ON ANTENNAS AND PROPAGATION in 2008 and 2012, the 2014 Piergiorgio Uslenghi Best Paper Award from the IEEE ANTENNAS AND WIRELESS PROPAGATION LETTERS, the 2015 IEEE John Kraus Antenna Award, and the 2018 Research Leader Award from the Faculty of Applied Science and Engineering, University of Toronto. He has served as the General Chair for the 2010 IEEE International Symposium on Antennas and Propagation held in Toronto. He has been serving as an Associate Editor for the IEEE TRANSACTIONS ON ANTENNAS AND PROPAGATION.